PHOSPHONATE FUNCTIONALIZED INORGANIC-ORGANIC HYBRID HYDROGELS FOR BONE REGENERATION

An Undergraduate Research Scholars Thesis

by

SARAH K. JONES

Submitted to the Undergraduate Research Scholars program at
Texas A&M University
in partial fulfillment of the requirements for the designation as an

UNDERGRADUATE RESEARCH SCHOLAR

Approved by Research Advisor: Dr. Melissa Grunlan

May 2019

Major: Biomedical Engineering

TABLE OF CONTENTS

Page

ABSTRACT 1

ACKNOWLEDGMENTS 2

LIST OF FIGURES 3

LIST OF TABLES 4

CHAPTER

I. INTRODUCTION 5

II. MATERIALS AND METHODS 8

- Materials 8
- Polymer Synthesis 8
- Polymer Characterization 11
- Hydrogel Fabrication 11
- Hydrogel Characterization 13

III. RESULTS AND DISCUSSION 17

- Polymer Synthesis 17
- Scaffold Composition Verification 19
- Scaffold Material Characterization 20

IV. CONCLUSION 27

REFERENCES 30

APPENDIX 33

ABSTRACT

Phosphonate Functionalized Inorganic-Organic Hybrid Hydrogels for Bone Regeneration

Sarah K. Jones
Department of Biomedical Engineering
Texas A&M University

Research Advisor: Dr. Melissa Grunlan
Department of Biomedical Engineering
Texas A&M University

Studies have indicated that the physical and chemical properties of scaffolds alone, without exogenous growth factors, can guide mesenchymal stem cell differentiation toward bone tissue regeneration. Ceramics, containing inorganics and phosphonates, are primarily used to impart osteoinductivity and bioactivity. However, these materials are brittle in nature which may lead to post-surgical fracture. Our lab has previously demonstrated osteoinductivity and bioactivity in a non-brittle, interconnected macroporous system with the presence of methacrylated star poly(dimethylsiloxane) ($PDMS_{star}$-MA) within a normally biologically inert poly(ethylene glycol) (PEG-DA) hydrogel. Because phosphorus-containing materials are known to increase osteoblastic differentiation and facilitate mineralization, this study aims to enhance this scaffold through functionalization of the inorganic $PDMS_{star}$-MA component with a phosphonate group. This was accomplished through the development and inclusion of a novel polymer, phosphonate-containing PPMS-DA. Key material properties were evaluated (i.e. modulus, swelling, degradation and bioactivity) and compared to a PEG-DA hydrogel and the previously studied hybrid hydrogel, PDMS:PEG. The phosphonate results indicated a more uniform distribution, similar mechanical properties and bioactivity, and increased degradation rate useful to promote tissue infiltration.

ACKNOWLEDGEMENTS

I would like to thank Prof. Melissa Grunlan, my primary research advisor, Michael Frassica, my graduate student mentor, and Jakkrit Suriboot, my synthesis advisor, for guiding me through this research project. They have driven me to perform to my highest potential and encouraged me in my pursuit of a research career. This project would not be possible without them.

I would also like to thank Texas A&M University for providing me this opportunity through the LAUNCH program and their support of undergraduate research.

Finally, I would like to thank my friends and family for supporting me through the course of this project. They have provided me with the encouragement and guidance necessary to complete this project.

LIST OF FIGURES

Page

Figure 1. PPMS-DA synthesis utilizes ring-opening polymerization, thiolene click chemistry, deprotection, and acrylation 8

Figure 2. Hydrogel fabrication utilizes salt template molding..... 11

Figure 3. PPMS-DA synthesis reaction 1, ring opening polymerization..... 16

Figure 4. PPMS-DA synthesis reactions 2, 3, and 4: thiol-ene click, deprotection, and thiol-ene click. 17

Figure 5. PPMS-DA synthesis reaction 5, diacrylation reaction 18

Figure 6. CLSM imaging reveals uniform distribution of PPMS-DA..... 19

Figure 7. The scaffolds' storage modulus was evaluated via DMA 20

Figure 8. Equilibrium swelling ratio was analyzed using two different methods..... 21

Figure 9. Degradation profile was analyzed via sacrificial mass loss... 22

Figure 10. Hydrophobicity was analyzed using DI water and IPA 23

Figure 11. SEM imaging reveals mineralization after SBF soak..... 24

Figure 12. Mineralized scaffolds' storage modulus was evaluated with DMA..... 25

Figure A1. DSC data for each reaction involved in PPMS-DA synthesis..... 32

Figure A2. NMR corresponding to reaction 1 of PPMS-DA synthesis..... 32

Figure A3. NMR corresponding to reaction 2 of PPMS-DA synthesis..... 33

Figure A4. NMR corresponding to reaction 3 of PPMS-DA synthesis..... 33

Figure A5. NMR corresponding to reaction 4 of PPMS-DA synthesis..... 34

Figure A6. NMR corresponding to reaction 5 of PPMS-DA synthesis..... 34

Figure A7. Mineralization topography was analyzed with SEM..... 35

LIST OF TABLES

Page

Table A1. Glass transition temperature for the product of each reaction involved in the PPMS-DA synthesis 36

Table A2. Sol content less than 5% verified successful crosslinking 36

CHAPTER I

INTRODUCTION

The loss of bone tissue due to disease, injury or congenital defect is a major medical problem with potential to be addressed by tissue engineering. The goal of tissue engineering is to assemble functional constructs that restore, maintain, or improve tissue function.[1] Conventionally, tissue engineering requires the integration of scaffolds, signals, and cells where the scaffolds will mimic the natural environment, signals will induce cell differentiation, and cells will differentiate into the desired tissue.[1] Typically, signals involve the use of growth factors that can induce cell differentiation and tissue growth, but high concentrated doses are required to maintain these effects.[2] This risks off-target responses and can be quite costly. Therefore, a "materials-guided approach" to regeneration - relying exclusively on the physical and chemical properties of the scaffold to guide cell differentiation – is desirable for tissue engineering.[3] Specifically, for bone tissue engineering, the material properties of the scaffold must promote bioactivity (i.e. promote the formation of hydroxyapatite (HAp) to allow interfacial bonding with surrounding tissue), osteoinductivity (i.e. promote differentiation of progenitor cells to an osteoblastic lineage), and osteoconductivity (i.e. support bone growth and ingrowth of surrounding bone).[4]

Inorganic materials containing ions of Si, P, and Ca such as bioactive glasses and ceramics are known to be both osteoinductive and bioactive.[5] However, there are several characteristics that hinder the use of these materials as regenerative scaffolds. For instance, while these materials have high compressive strength, they also have a weak fracture toughness inhibiting their load bearing capacity.[6] Finally, the rate of degradation is much slower than ideal, and therefore hampers

neotissue growth.[7] Thus, a scaffold that overcomes these issues while maintaining an osteoinductive and bioactive nature would be an ideal strategy for bone tissue engineering.

Recently, our lab has developed a hybrid scaffold to mitigate these issues consisting of crosslinked inorganic poly(dimethylsiloxane) star methacrylate ($PDMS_{star}$-MA) and organic poly(ethylene glycol) diacrylate (PEG-DA).[8] PEG-DA hydrogels have been used frequently in tissue engineering because of their inherent resistance to protein adsorption and cell adhesion.[9] Further, the UV-curable functionality supports a variety of fabrication methods and the inclusion of cell-adhesive ligands (i.e. RGDS) for controlled cell adhesion. It has been determined that this inorganic-organic hybrid material maintains controlled cell adhesion while gaining osteoinductivity and bioactivity.[10] While improving upon the previously mentioned $PDMS_{star}$-MA containing PEG-DA hydrogel, our lab incorporated both solvent induced phase separation (SIPS) and fused salt templating into their fabrication.[11, 12] While SIPS was initially introduced to improve $PDMS_{star}$-MA dispersion, it allowed the use of salt with a dichloromethane (DCM) based precursor. Fused salt templating introduced an interconnected macroporous structure that is easily tunable to the ideal pore size for bone tissue growth (i.e. 200-400μm) throughout the scaffold.[13]

We now aim to further enhance the osteoinductive and bioactive nature of this hydrogel scaffold with the addition of a phosphonate side group. Phosphate is found naturally at the site of bone regeneration in the form of hydroxyapatite. This presence has led to the investigation of phosphorus-containing polymers for bone regeneration. It has been determined that the presence of a pendant phosphate group increased both mineralization and osteoblast differentiation/proliferation.[14] Considering the osteoinductivity and bioactivity induced by the inorganic presence in our PDMS-PEG hydrogel, the introduction of a phosphonate side group to PDMS is expected to further enhance its osteoinductive and bioactive capacity. Therefore, we aim

to develop a novel polymer, diacrylated polydiethyl(2-(propylthio)ethyl)phosphonate methylsiloxane (PPMS-DA), to introduce into the PEG-DA matrix in the place of $PDMS_{star}$-MA. To determine the phosphonate group's effect, we will determine the material characteristics of the scaffold (i.e. morphology, modulus, swelling and degradation) and *in vitro* bioactivity. All tests will be conducted using a PEG-DA hydrogel and a 20:80 PDMS:PEG hybrid hydrogel as controls, and the scaffold fabrication method used for the phosphonate functionalized PDMS:PEG hydrogels will be adopted from that of the PDMS:PEG hybrid hydrogels.

CHAPTER II

MATERIALS AND METHODS

Materials

1-vinyl-2-pyrrolidinone (NVP), 2,2'-azobis(2-methylpropionitrile) (AIBN), 2,2-dimethyl-2-phenylacetophenone (DMAP), acryloyl chloride, allyl methacrylate, calcium chloride, dibasic potassium phosphate, diethyl vinylphosphonate, HCl, hexamethyldisilazane (HMDS), magnesium chloride hexahydrate, magnesium sulfate, NaOH, Nile red, NMR grade, deuterated chloroform ($CDCl_3$), poly(ethylene glycol) 3350 (PEG-3350), potassium carbonate, potassium chloride, silica gel, sodium bicarbonate, sodium chloride (salt), sodium sulfate, thioacetic acid, triethylamine, trifluoromethanesulfonic acid (triflic acid), tris-hydroxymethyl aminomethane, and all solvents were obtained from Sigma-Aldrich. 1,3,5,7-tetravinyl-1,3,5,7-tetramethylcyclotetrasiloxane, 1,3-bis(4-hydroxybutyl)tetramethyldisiloxane (HBTMDS), HPLC-grade toluene, dichloromethane (DCM), and NMR grade $CDCl_3$ were dried over 4 Å molecular sieves. Salt was sifted (ASTM E11 Specification, No. 40, 425 μm opening; No. 60, 250 μm opening) to obtain 268 ± 35 μm salt. Octamethylcyclotetrasiloxane (D4), Pt-divinyltetramethyldisiloxane complex in 2 wt% xylene (Karstedt's catalyst), and tetrakis(dimethylsiloxy)silane (tetra-SiH) were obtained from Gelest. Activated carbon was obtained from Fisher Scientific.

Polymer Synthesis

PPMS-DA Synthesis

All reactions contained a Teflon covered stir bar to agitate the reaction mixture, diacrylated poly(diethyl(2-(propylthio)ethyl)phosphonate methylsiloxane) (PPMS-DA) was prepared in five synthetic steps as outlined in **Figure 1**.

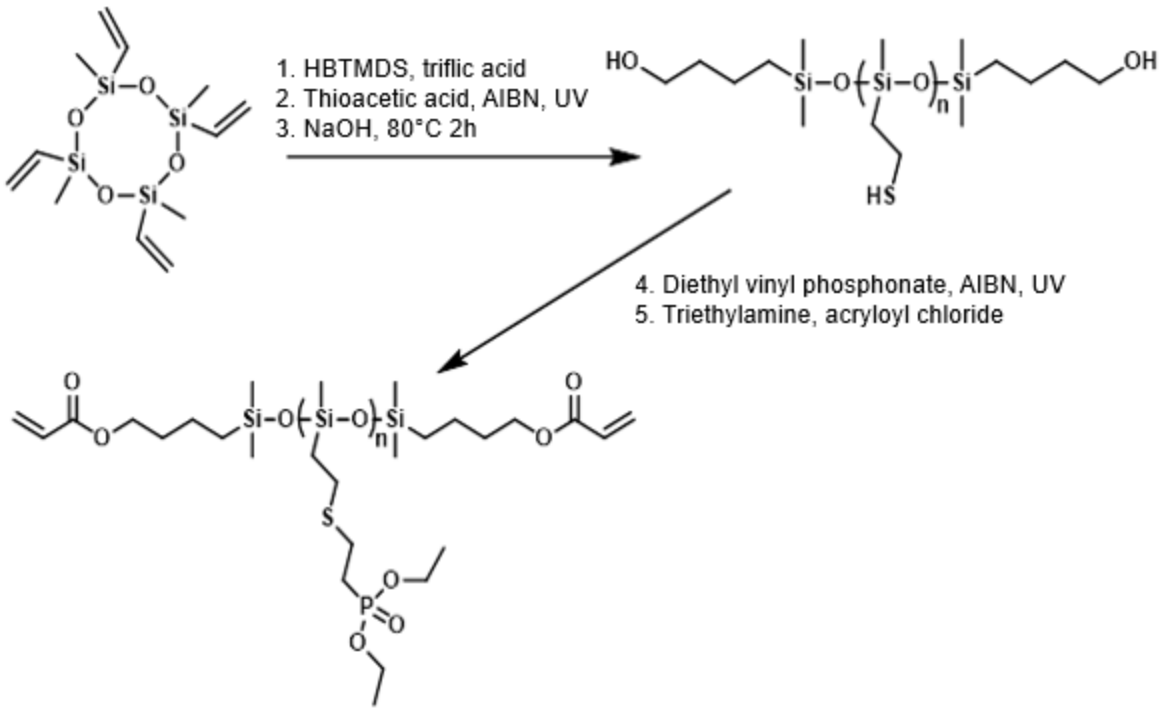

Figure 1. PPMS-DA synthesis utilizes ring-opening polymerization, thiolene click chemistry, deprotection, and acrylation.

First, molecule B was prepared by the acid catalyzed equilibration of 1,3,5,7-tetravinyl-1,3,5,7-tetramethylcyclotetrasiloxane (15 g; 43.5 mmol) with 4.85 g molecule A (HBTMDS) (4.85 g; 17.4 mmol). These reagents were combined in a 50 mL round bottom flask equipped with a rubber septum and triflic acid (60 µL; 0.678 mmol) added via syringe. The mixture was allowed to stir 12 h at 75°C then HMDS (194 µL; 0.930 mmol) was added to neutralize the mixture. The polymer mixture was precipitated in a 1:1 methanol to water solution to isolate molecule B.

Second, molecule C was prepared via thiolene click chemistry by combining thioacetic acid (9.38 mL; 131.1 mmol) and AIBN (.289 g; 1.75 mmol) with molecule B (11 g; 9.62mmol) in a 50 mL round bottom flask equipped with a rubber septum. The mixture was allowed to stir overnight at room temperature (RT) under UV light (2mW/cm^2, 365nm). Molecule C was precipitated as done in the previous step.

Third, molecule D was prepared via deprotection with NaOH at 85°C. Ethanol (85 mL) was added to molecule C (15 g; 6.99 mmol), and water (21 mL) was added to NaOH (6.12 g; 157.4 mmol) separately. The two solutions were combined in a 500 mL round bottom flask in a typical reflux apparatus for 2 h at 80°C. 2M HCl (100 mL) was added to neutralize the solution. The solution was transferred into a 1000 mL separatory funnel. Molecule D was precipitated in ether (200 mL) and washed with water (2 x 100 mL) and brine (1 x 100 mL), each time removing the aqueous layer to isolate molecule D.

In the fourth step, molecule E was prepared via thiolene click chemistry by combining diethyl vinyl phosphonate (10.49 g; 63.91 mmol) and AIBN (0.113 g; 0.688 mmol) with molecule D (7 g; 3.92 mmol) in a 50 mL round bottom flask equipped with a rubber septum. The mixture was allowed to stir overnight at RT under UV light (2mW/cm^2, 365nm). The polymer mixture was precipitated in a 1:1 water to methanol solution to isolate molecule E.

In the fifth step, molecule F was prepared by acrylating the terminal hydroxyl groups of molecule E. Molecule E (7 g; 1.97 mmol) was dissolved in DCM (35 mL) in a 100 mL round bottom flask round bottom flask equipped with a rubber septum. Et_3N (0.548 mL; 3.94 mmol) and acryloyl chloride (0.640 mL; 7.88 mmol) were sequentially added dropwise via syringe. The reaction mixture was allowed to stir at RT overnight. Molecule F was dissolved in DCM (100 mL), precipitated in 2M K_2CO_3 (10 mL), and washed with water (10 mL). The organic layer was removed and precipitated in a 1:1 water to methanol solution to isolate molecule F.

$PDMS_{star}$-MA Synthesis

$PDMS_{star}$-MA (2k g/mol) was prepared as previously reported.[8]

PEG-DA Synthesis

PEG-DA (3.4k g/mol) was prepared as previously reported.[8]

Polymer Characterization

Nuclear Magnetic Resonance (NMR)

^{1}H-NMR spectra were obtained on an 'INOVA 500' 500 MHz spectrometer operating in the Fourier transform mode. Five percent (w/v) $CDCl_3$ solutions were used to obtain spectra. Residual $CHCl_3$ served as an internal standard.

Differential Scanning Calorimetry (DSC)

DSC (TA Instruments Q100) was used to determine the Tg of each molecule obtained throughout the synthesis of PPMS-DA. Sample analysis was performed with ~10-15 mg sealed in a hermetic pan. The sample was cooled at a rate of 5°C min^{-1} from 25 to -180°C then heated at a rate of 5°C min from -180 to 0°C. The Tg was characterized as the midpoint of the sudden increase in heatflow.

Hydrogel Fabrication

Mold Construction

One end of a borosilicate glass tube (5/8" OD, 1/2" ID, 1.5" H) was capped with aluminum foil. The foil side of the tube was placed into a custom Teflon cap (1" OD, 5/8" ID) that contained a small hole (0.05" D) through its center. The excess foil was pushed down toward the cap so as not to go up the sides of the tube. The mold was wrapped tightly in Parafilm to ensure no movement between the tube and the cap, and the Parafilm was pushed down towards the cap so as not to inhibit travel of UV-light through the mold.

Salt Templating

Salt (268 ± 35 μm) was mixed with 5 wt% DI water to form a slurry of which 3.5 g was placed into the mold. The salt was slightly compressed using a flat-ended glass rod to form a cylindrical construct in the glass mold. The tube was covered in Parafilm, and centrifuged for 5

min at 2000 rpm (Eppendorf 5810R centrifuge, A-4-62 rotor). The Parafilm cap was removed and the salt templates were allowed to air dry at RT for 24 h as seen in **Figure 2**.

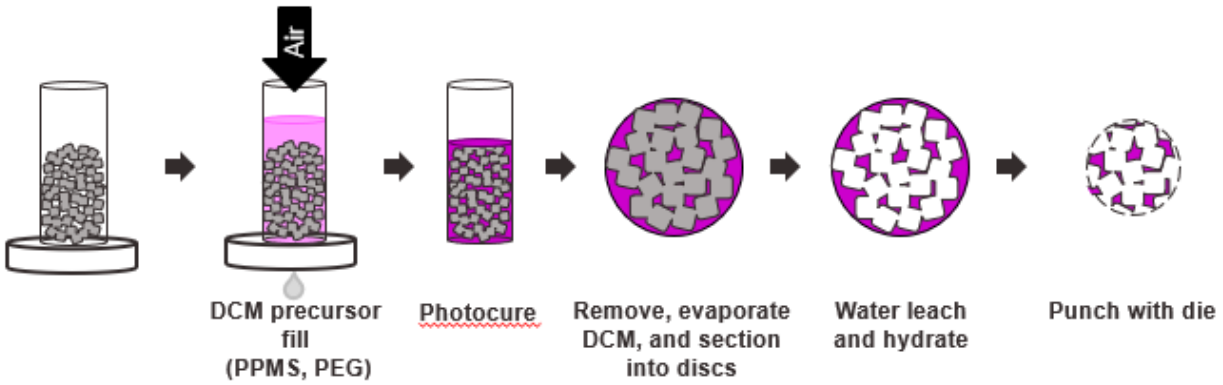

Figure 2. Hydrogel fabrication utilizes salt template molding.

Templated Hydrogel Fabrication

DCM-based precursor solutions were prepared containing 30 wt% total macromer (based on total solution mass) with increasing wt% ratios of PPMS-DA to PEG-DA: 0:100 (PEG-DA control), 10:90, 20:80, and 30:70. A 20:80 $PDMS_{star}$-MA:PEG-DA solution was also prepared ($PDMS_{star}$-MA control). A photoinitiator solution of 30 wt% DMP in NVP was added at 0.1 mL/g of macromer. During preparation, solutions were vortexed for 1 min after each addition. The final precursor solution was immediately added to the prepared salt template via syringe after vortexing. After equilibration in the salt template, the foil at the base of the mold was punctured through the hole in the Teflon cap via paper clip. PVC tubing (3/8" ID, 9/16" OD) was pressed against the top opening of the mold, and compressed air was used to force the solution through the salt template until it began to exit through the hole in the base of the mold as seen in **Figure 2**. The mold was then immediately placed on a UV plate (UV-transilluminator; 6 mW cm^2, 365 nm) and covered with a foil wrapped beaker for 15 min (12 min sitting on Teflon cap, 3 min on glass tube).

The template was allowed to air dry for 24 h before being removed from the mold via a flat-ended glass rod and cut into 1.2 mm thick discs using a vibratome (Leica VT1000S) with a

cutting speed of 1.75 mm/s and a frequency of 30 Hz. The top and bottom 4 mm of the cylinder were discarded and not used for testing. Discs were placed in scintillation vials containing 17 mL DI water, and placed on a rocker table at 100 rpm for 48 h. The DI water was exchanged three times a day to leach salt and swell the hydrogels. The discs were placed in fresh DI water and allowed to soak for an additional 72 h before testing. For testing, each disc was punched to either 8 or 13 mm diameter from the center of the disc using a die.

Hydrogel Characterization

Sol Content

Six hydrogels of each composition (PEG, 20:80 2k PDMS, 10:90 PPMS, 20:80 PPMS, and 30:70 PPMS) were cut into 13 mm discs. Each disc was allowed to air dry for 30 min in an open scintillation vial and then placed in a vacuum oven for 24 h (RT, 14.7 psi). Each disc was weighed (W_{d1}) and placed in a new scintillation vial with 10 mL DCM for 48 h on a rocker table at 200 rpm. Following the soak, the discs were placed in a new empty scintillation vial. Each disc was allowed to air dry for 30 min in an open scintillation vial and then placed in vacuum oven for 24 h at RT and 14.7 psi. Finally, each disc was weighed (W_{d2}) and sol content was calculated as $[(W_{d1}-W_{d2})/W_{d1}]*100$.

Confocal Imaging

A Nile Red solution was prepared by mixing 75 µL of a solution of 20 mg Nile Red and 1 mL methanol with 8 mL DI water and adding to 120 mL PBS. One hydrogel of each composition was cut into an 8 mm disc and soaked in the Nile Red solution for 24 h. Each sample then underwent three days of PBS soak with daily changes. An Olympus FV1000 confocal microscope, equipped with a UPLSAPO 10x/0.4 objective, was used to capture an image of the stained discs, which were placed in a coverglass-bottom chamber. Excitation and emission were 488 nm and

500-600 nm, respectively. The confocal aperture was set to 1 Airy unit. Z-stacks (80 slices) were acquired with a 4.0 µm step. Confocal zoom and resolution setting resulted in XY pixel size of 2.485 µm. Representative slices of the stacks were exported. The fluorescence images were pseudo-colored green. Bright field imaging was conducted simultaneously.

Scanning Electron Microscopy (SEM)

One hydrogel of each composition was cut into a 8 mm disc. Each disc was placed in an open scintillation vial and allowed to air dry for 30 min before being placed in a vacuum oven for 24 h at RT and 14.7 psi. Dried discs received an Au-sputter coating via a Cressington Sputter Coater 108. Coated discs were imaged using a field emission scanning electron microscope (JEOL NeoScope JCM-5000) at an accelerated electron energy of 10keV. Each hydrogel was imaged at 100x magnification. This was completed before and after soaking in SBF.

Dynamic Mechanical Analysis (DMA)

Storage modulus was measured using a DMA (TA Instruments Q800) with parallel plate compression. Six hydrogels of each composition were cut into 8 mm discs. Each disc was placed in the center of the bottom plate (40 mm diameter). Two or three drops of DI water were pipetted on the top of the disc to encase the disc in water. The top plate (15 mm diameter) was lowered onto the disc. Samples were tested at RT using a multi-frequency strain mode (1-30Hz).

Equilibrium Swelling

Eight hydrogels of each composition were cut into 13 mm discs, placed into scintillation vials with 15 mL DI water, and placed on a rocker table at 200 rpm for 48 h. Each disc was removed from water and immediately weighed (W_s). The disc was placed on a stack of 4 KimWipes for 3 seconds then flipped for 3 seconds and weighed again (W_w). After weighing, each disc was placed into a new scintillation vial, allowed to air dry for 30 min, and placed into a vacuum oven at 60°C

and 14.7 psi for 24 h. Each disc was removed from the oven and weighed (W_d). Conventional equilibrium swelling was calculated as $(W_s-W_d)/W_d$, and a separate swelling value to correct for porosity was calculated as $(W_w-W_d)/W_d$.

Accelerated Degradation

Accelerated degradation analysis was conducted by the following sacrificial mass loss procedure. Six hydrogels of each composition were cut into 8mm discs and placed into individual 1 dram vials. Each vial was placed into a vacuum oven at RT and 14.7 psi for 24 h. Each disc was removed from the vacuum oven and weighed (W_1). After weighing, each disc was placed into a new 1 dram vial with 1mL 0.05M NaOH. Each vial was placed into a shaking incubator at 37°C and 100 rpm. Every 12 h the solution was removed and replaced with 1mL 0.05M NaOH. At 12 h time points, one disc of each composition was removed and dried at RT and 14.7psi for 12 h then weighed (W_2). This was repeated for the following 72 h. Mass loss was calculated at each time point as $[(W_1-W_2)/W_1]*100$. This procedure was followed 3 times to obtain a graphical representation of mass loss.

Hydrophobicity-Index

Eight hydrogels of each composition were cut into 13mm discs, placed into scintillation vials, and placed into a vacuum oven at RT and 14.7 psi for 48 h. Each disc was removed from the oven and weighed (W_d). Four hydrogels of each composition were subsequently placed into scintillations vials with 10mL of DI water and the remaining four were placed into scintillation vials with 10mL of aqueous 70% isopropanol. All vials were placed onto a rocker table at 200 rpm for 36 h. Each disc was then weighed (Ws). The swelling ratio of each disc was calculated by $q_k=(W_s/W_d)$ with k being either ‘h2o’ for DI water or ‘ipa’ for isopropanol. The H-index was then calculated by $H=(q_{ipa}/q_{h2o})$ for each pair (DI water and IPA) in each composition.

Simulated Body Fluid Soak

Eight hydrogels of each composition were cut into 8mm discs and placed flat at the bottom of a conical 50 mL centrifuge tube containing 40 mL of simulated body fluid (SBF). The SBF solution was fabricated as detailed by *Kokubo et al*.[15] Tubes were placed in a water bath at 37°C for 4 weeks. Each disc was then rinsed with DI water and vacuum dried at RT and 14.7psi for 24 h. Dried hydrogels were subjected to SEM imaging.

Statistical Analysis

Data is reported as the mean ± standard deviation. Data set mean values were compared in GraphPad Prism via ANOVA followed by Tukey's posthoc test where p-value < 0.05 was considered statistically significant.

CHAPTER III

RESULTS AND DISCUSSION

Polymer Synthesis

Phosphorus-containing materials are known to increase osteoblastic differentiation and facilitate mineralization.[14] Additionally, phosphorus is prevalent within the natural bone matrix as a primary component of hydroxyapatite, the inorganic component of bone tissue.[16] Therefore, this study aims to enhance the osteogenic capacity of the previous $PDMS_{star}$-MA:PEG-DA hybrid hydrogel by functionalizing the siloxane backbone with a pendant phosphonate group.

The synthesis of this novel polymer, diacrylated polydiethyl(2-(propylthio)ethyl)phosphonate methylsiloxane (PPMS-DA), is a five-step process that results in the formation of a diacrylated siloxane polymer with a phosphonate pendant group. For the first reaction, a ring opening polymerization was performed with 1,3,5,7-tetravinyl-1,3,5,7-tetramethylcyclotetrasiloxane (D4 vinyl) and 1,3-bis(4-hydroxybutyl)tetramethyldisiloxane (HBTMDS) as seen in **Figure 3**. HBTMDS was chosen because it contains a four-carbon separated hydroxyl end group, which is stable and will remain stable in the succeeding reactions. The hydroxyl end group can also be converted into a diacrylate end group for crosslinking after the addition of the side group.

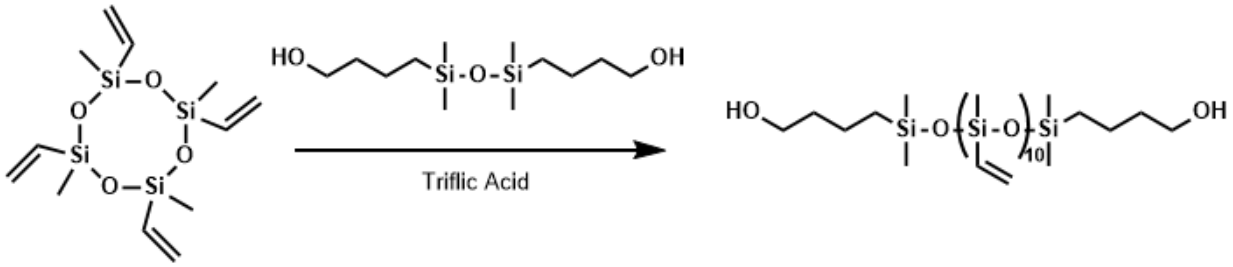

Figure 3. PPMS-DA synthesis reaction 1, ring opening polymerization.

For the second reaction, thioacetic acid was added to enable a back to back thiol-ene click reaction to ultimately add the phosphonate group. Thioacetic acid provided a facile route to conduct a controlled thiol-ene click reaction via a protected thiol, that could then be deprotected with a base catalyzed reflux reaction and subsequently used in a separate thiol-ene click reaction to facilitate the addition of the phosphonate group as seen in **Figure 4**.

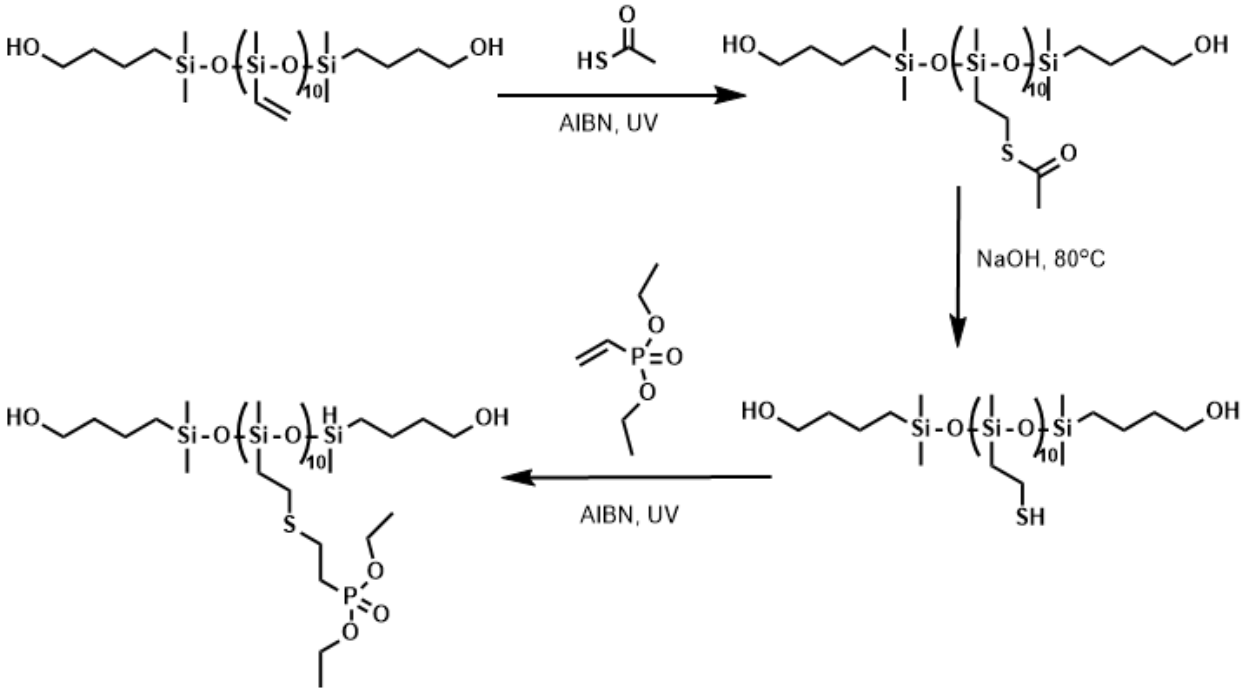

Figure 4. PPMS-DA synthesis reactions 2, 3, and 4: thiol-ene click, deprotection, and thiol-ene click.

Since the reactive thiol is eventually stabilized by binding it between the siloxane backbone and the stable phosphonate group, acryloyl chloride can be used to convert the hydroxyl end groups to diacrylate end groups without disturbing the polymer, as seen in **Figure 5**. This will facilitate the crosslinking of PPMS-DA with PEG-DA in the hydrogel matrix. After each reaction was performed, an NMR and DSC were both evaluated to confirm the structure of the resulting polymer; these can be found in **Figures A1-6** and **Table A1** of the appendix.

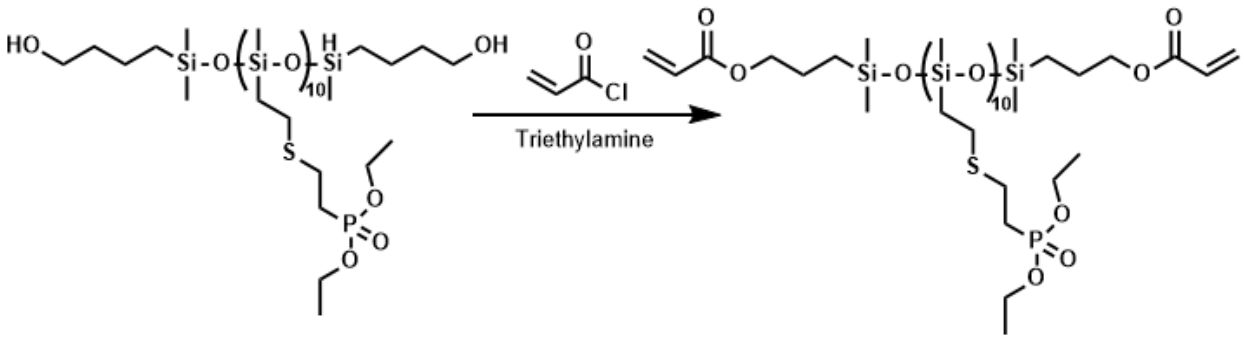

Figure 5. PPMS-DA synthesis reaction 5, diacrylation reaction.

Scaffold Composition Verification

The PPMS-DA:PEG-DA hybrid hydrogel scaffold was fabricated using the same method as the $PDMS_{star}$-MA:PEG-DA hybrid hydrogel scaffold to allow for appropriate comparison between the two materials. This includes solvent induced phase separation (SIPS) and fused salt templating.[11, 12] Following fabrication, a sol content value less than 5% for all concentrations of PPMS-DA containing hydrogel scaffolds was used to provide sufficient evidence to confirm the successful crosslinking between the PPMS-DA and PEG-DA within the hydrogel matrix. This data can be found in **Table A2** of the appendix.

Additionally, the PPMS-DA was stained within the hydrogel scaffold using Nile Red stain and fluorescent imaged by confocal scanning laser microscopy (CLSM) as seen in **Figure 6**. The green seen in these images reflects distribution of the PPMS-DA throughout the hydrogel scaffold because the hydrophobic Nile Red stains the hydrophobic siloxane in the hydrogel. The $PDMS_{star}$-MA was also stained green within the hydrogel scaffold and imaged similarly. The $PDMS_{star}$-MA images revealed small bright green areas within the hydrogel scaffold which reflects an uneven distribution of $PDMS_{star}$-MA within the scaffold. This can be attributed to the poor miscibility of $PDMS_{star}$-MA within the precursor solution, which was cloudy prior to curing. However, the PPMS-DA images did not reflect any bright areas and thus exhibited a uniform distribution. This can be attributed to the increased miscibility of PPMS-DA within DCM that was observed in a

clear precursor solution as compared to $PDMS_{star}$-MA. Having a uniform distribution of PPMS-DA within the hydrogel scaffold will provide for more uniform material properties which is favorable for maximum and consistent cell signaling.

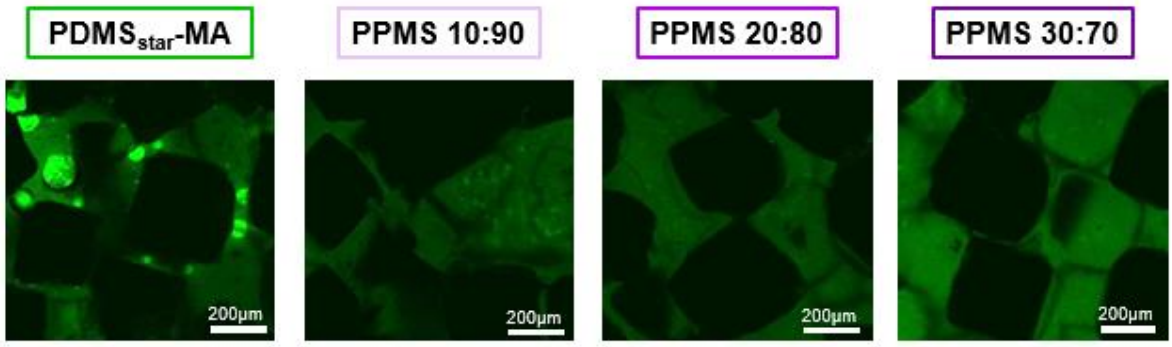

Figure 6. CLSM imaging reveals uniform distribution of PPMS-DA. Green represents the hydrophobic areas stained with Nile Red, either PPMS-DA or $PDMS_{star}$-MA. Scale bars = 200µm.

Scaffold Material Characterization

Storage Modulus

Because a scaffold's storage modulus (a measure of the elastic response of a material) is known to effect the surrounding cellular response, it was evaluated using Dynamic Mechanical Analysis (DMA). [17] Storage modulus was examined for increasing concentrations of PPMS-DA containing hydrogels and compared to both a PEG-DA control and a $PDMS_{star}$-MA control. The results indicated that the PPMS-DA scaffolds exhibit a statistically significant increase in storage modulus as compared to the PEG-DA control, and a similar storage modulus as compared to the $PDMS_{star}$-MA control as seen in **Figure 7**. Though similar to the $PDMS_{star}$-MA containing hydrogel, the exhibited storage modulus of the PPMS-DA scaffolds is within the range known to promote osteogenesis (11-30kPa).[17, 18] Based on its chemistry, the bioactivity and osteoinductivity of the PPMS-DA scaffold is expected to further increase the apparent modulus through mineralization and eventual neotissue support.

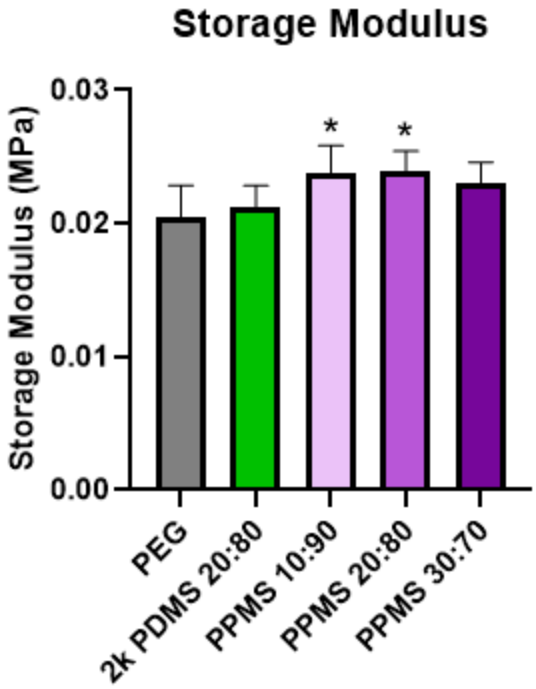

Figure 7. The scaffolds' storage modulus was evaluated via DMA. Storage modulus of PPMS-DA hydrogels is within optimal range for osteogenesis.

Hydrophobicity

Since hydrophobicity is known as an osteoinductive scaffold property, the equilibrium swelling ratio was examined for increasing concentrations of PPMS-DA containing hydrogels and compared to both a PEG-DA control and a $PDMS_{star}$-MA control.[19] Two procedures were followed to examine the swelling ratio, the first being the conventional procedure of obtaining the swollen weight by taking the hydrogel right out of the water and weighing. The second procedure corrected for the porosity by wicking water from the interconnected pores.

The conventional method to measure equilibrium swelling, without correcting for porosity, showed a statistically significant increase in hydrophobicity for PPMS-DA hydrogels compared to the PEG-DA control and a similar hydrophobicity to the $PDMS_{star}$-MA control as seen in the left graph in **Figure 8**. However, the varying concentrations of PPMS-DA all maintained similar values of swelling as well.

Using the method that corrected for porosity, the 20:80 and 30:70 PPMS-DA hydrogel scaffolds exhibited a statistically significant increase in hydrophobicity relative to the PEG-DA control and similar hydrophobicity to the $PDMS_{star}$-MA control. However, the 10:90 PPMS-DA hydrogel scaffold had similar values to the PEG-DA control as seen in the right graph in **Figure 8**. This data indicates that the increasing concentration of PPMS-DA in the primarily PEG-DA hydrogel slowly increases the hydrophobicity of the scaffold. This enables the scaffold to have tunable hydrophobicity with controlled concentrations of PPMS-DA.

However, the large presence of interconnected macropores is a source of inaccuracy in measuring the water affinity of the PPMS-DA hydrogel scaffolds, so further studies will be conducted using non-templated PPMS-DA:PEG-DA hydrogels without interconnected macropores to better evaluate the water affinity of the material.

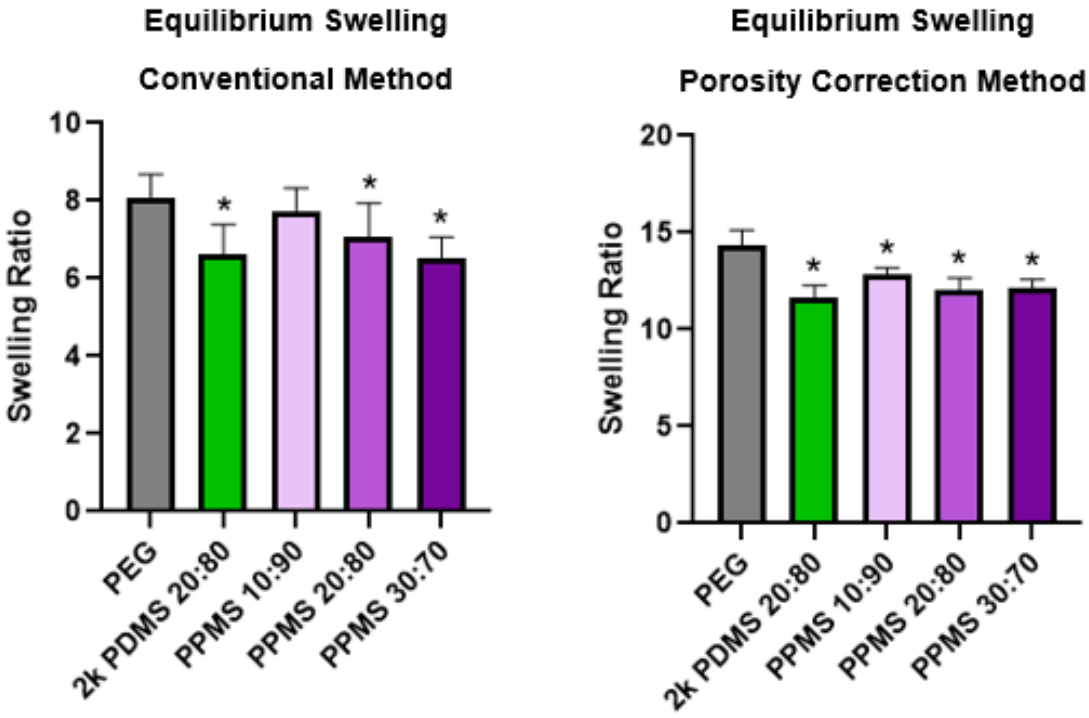

Figure 8. Equilibrium swelling ratio was analyzed using two different methods. The conventional method and a method to mitigate the error caused by macroporosity. PPMS-DA hydrogels had increased hydrophobicity compared to PEG-DA, and may be tunable by PPMS-DA concentration.

Degradation Profile

Lastly, the degradation profile was analyzed using a sacrificial mass loss procedure. The degradation rate, quantified by mass loss percentage, was evaluated for three increasing concentrations of PPMS-DA containing hydrogels and compared to both a PEG-DA control and a $PDMS_{star}$-MA control. The results indicated that the 20:80 and 30:70 PPMS-DA scaffolds have a significant increase in degradation rate starting at 36 h as compared to the PEG-DA and $PDMS_{star}$-MA controls. The 10:90 PPMS-DA scaffolds exhibited a similar degradation rate to the controls as seen in **Figure 9**. This data indicates that the increasing concentration of PPMS-DA in the primarily PEG-DA hydrogel increases the degradation rate of the scaffold. This enables the scaffold to have a tunable degradation profile with controlled concentrations of PPMS-DA. This is an important quality for bone regenerative scaffolds because the scaffold needs to degrade slow enough to provide a sufficient framework for neotissue growth, but degrade fast enough so as to not inhibit tissue proliferation.[1]

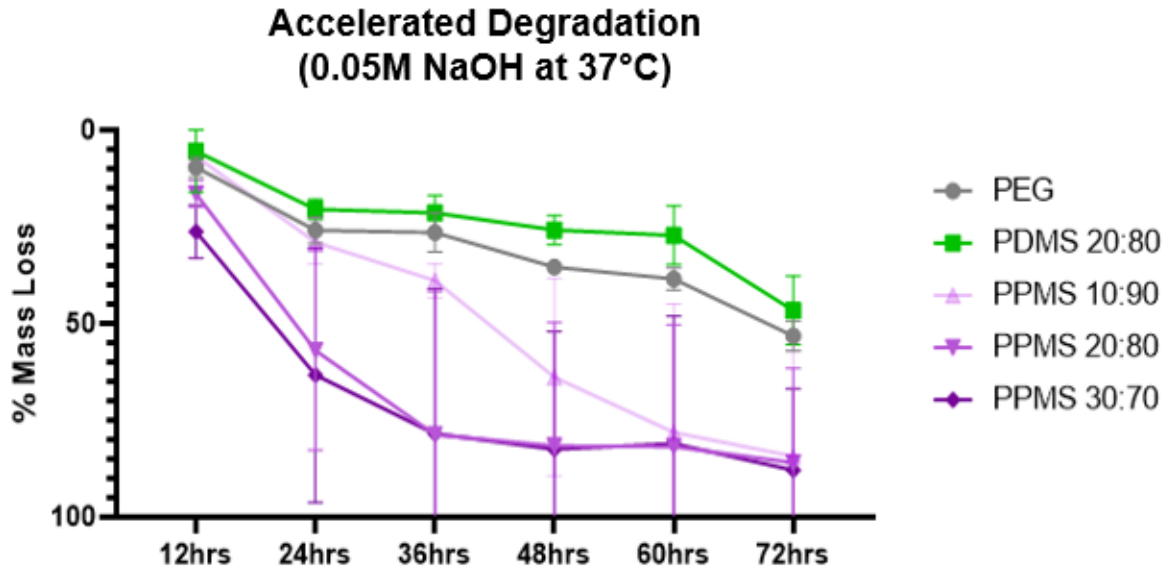

Figure 9. Degradation profile was analyzed via sacrificial mass loss. PPMS-DA hydrogels exhibited an increased degradation rate, tunable by PPMS-DA concentration.

Hydrophobicity-Index

In an effort to explain the increased degradation rate of the PPMS-DA containing hydrogels, an H-index test was run to evaluate the differences in relative hydrophobicity of the different hydrogel compositions. As seen in **Figure 10**, the results indicated that all of the PPMS-DA containing hydrogels along with the PEG-DA and $PDMS_{star}$-MA controls have relatively similar hydrophobicity levels. Therefore, the hydrophobicity of the PPMS-DA containing hydrogels does not explain the increased degradation rate. However, similar to the equilibrium swelling testing, this test method may be hindered by the large presence of pores in the scaffold. Further testing will be conducted with non-templated hydrogels in an effort to explain the increased degradation rate of the PPMS-DA containing hydrogels relative to the PEG-DA and $PDMS_{star}$-MA controls without the added sophistication of a porous scaffold. A potential area of interest is the possible hydrolysis of the phosphonate group accelerating the degradation process.

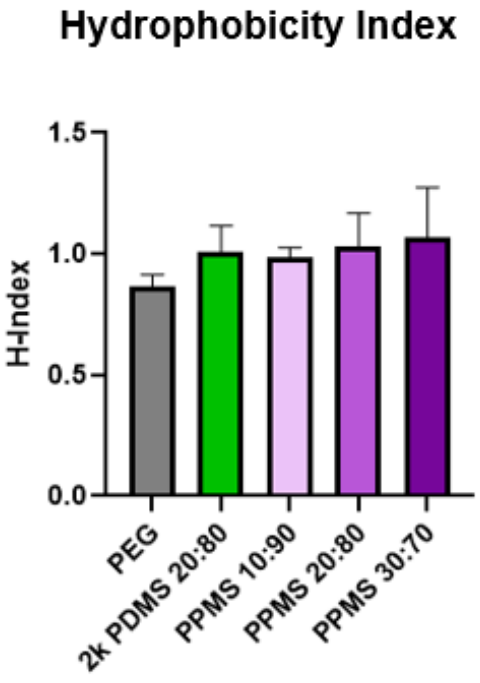

Figure 10. Hydrophobicity was analyzed using DI water and IPA. Resulted in similar hydrophobicity in all compositions.

Bioactivity

Bioactivity is a key property of bone regenerative scaffolds because it promotes bonding with adjacent bone tissue.[6] Therefore, the PPMS-DA containing hydrogels were subjected to a 4-week SBF soak and subsequently imaged with SEM. As seen in **Figure 11**, the results indicated that the PPMS-DA containing hydrogels supported mineralization after 4 weeks in an *in vitro* environment that is similar in ionic concentration, pH, and temperature to the intended implant environment. When compared to the controls, the PPMS-DA containing hydrogels supported more mineralization than the PEG-DA control and similar mineralization the $PDMS_{star}$-MA control. As expected, the PEG-DA control did not support mineralization and remained bare after the 4-week soaking period. The $PDMS_{star}$-MA control supported mineralization, and showed qualitatively similar mineralization to the PPMS-DA containing hydrogels. The mineralization of the PPMS-DA containing hydrogels indicates that the PPMS-DA increased the bioactivity of the otherwise inert PEG-DA hydrogel, similar to the $PDMS_{star}$-MA control.

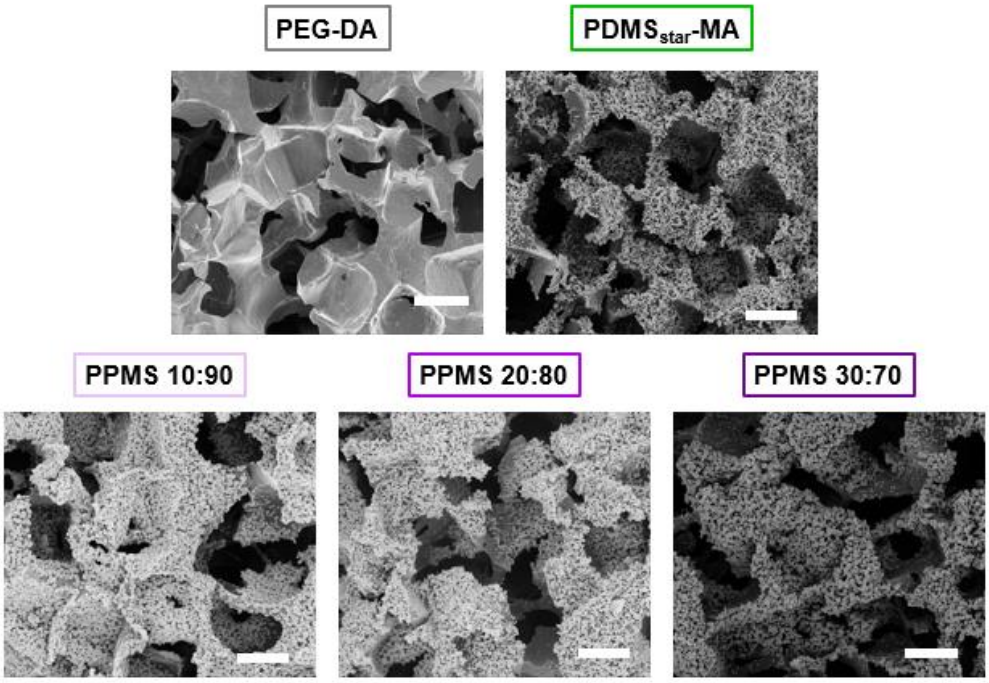

Figure 11. SEM imaging reveals mineralization after SBF soak. Scale bars = 200µm.

It is highly expected that the discovered mineralization is hydroxyapatite because of its apparent structure, spherical aggregates of crystals that are interwoven into a porous structure.[20] Mineralization structure can be seen in **Figure A7** of the appendix. Further investigation will need to be conducted with energy dispersive x-ray spectroscopy (EDS) to confirm the identity of the mineralization via chemical composition.[21]

Storage Modulus with Mineralization

Because the bioactivity of the PPMS-DA scaffold is expected to further increase the apparent modulus through mineralization, storage modulus was examined using DMA following the 4-week SBF soak that resulted in mineralization. As seen in Figure 12, the results indicated similar storage modulus values for each composition with and without mineralization, except the PPMS-DA 20:80 which exhibited a loss in storage modulus with mineralization. The lack of enhanced structural rigidity as a result of mineralization can be attributed to scaffold degradation during the 4-week soaking period in the SBF solution. Further evaluation will be conducted in order to determine the effect of mineralization on the structural rigidity of the hydrogel scaffolds.

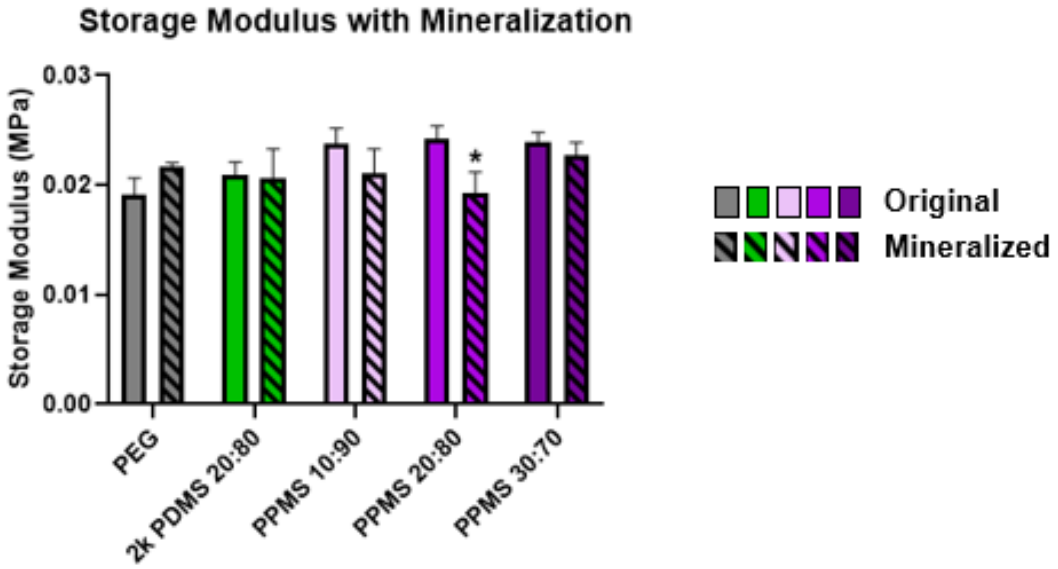

Figure 12. Mineralized scaffolds' storage modulus was evaluated with DMA. Storage modulus was not affected by mineralization.

CHAPTER IV

CONCLUSION

Research indicates that the physical and chemical properties of scaffolds alone, without exogenous growth factors, can guide mesenchymal stem cell behavior toward tissue regeneration.[3, 22, 23] Ceramics, containing inorganics and phosphonates, are primarily used to impart this osteoinductivity and bioactivity however are brittle in nature.[5, 6] Our lab has confirmed the osteoinductivity and bioactivity of a recently developed interconnected macroporous hybrid hydrogel scaffold consisting of crosslinked inorganic $PDMS_{star}$-MA and organic PEG-DA to mitigate the weak fracture toughness and slow degradation rate characteristic of ceramic scaffolds.[8] Therefore, we have functionalized the PDMS-MA component of a confirmed bioactive and osteoinductive hydrogel scaffold with a phosphonate pendant group to further optimize its bone regenerative capacity.

PPMS-DA was synthesized and crosslinked with PEG-DA into an interconnected macroporous hydrogel network in increasing ratios (10:90, 20:80, and 30:70) and compared to interconnected macroporous $PDMS_{star}$-MA and PEG-DA controls. The PPMS-DA containing hydrogels exhibited a more uniform distribution than the $PDMS_{star}$-MA control, which will facilitate more uniform scaffold properties to promote the appropriate cellular response.

Mechanical analysis revealed similar storage modulus and hydrophilicity in the PPMS-DA containing hydrogels compared to the $PDMS_{star}$-MA control. Though similar to the $PDMS_{star}$-MA containing hydrogel, the exhibited storage modulus of the PPMS-DA scaffolds is within the range known to promote osteogenesis.[17, 18]

Degradation analysis revealed a significant increase in degradation rate in the PPMS-DA containing hydrogels with increasing concentrations of PPMS-DA. This enables the scaffold to have a tunable degradation profile with controlled concentrations of PPMS-DA. This is an important quality for bone regenerative scaffolds because the scaffold needs to degrade slow enough to provide a sufficient framework for neotissue growth, but degrade fast enough to allow for tissue proliferation. Hydrophobicity analysis was conducted in an effort to explain the increased degradation rate, but results indicated a similar hydrophobicity for all compositions. Further investigation will be conducted to explain the significant change in the degradation profile due to the phosphonate functionalization. A potential area of interest is the possible hydrolysis of the phosphonate group accelerating the degradation process.

Lastly, bioactivity analysis revealed significant mineralization of the PPMS-DA containing hydrogels. The mineralization of the PPMS-DA containing hydrogels indicates that the PPMS-DA increased the bioactivity of the otherwise inert PEG-DA hydrogel, similar to the $PDMS_{star}$-MA control. Further investigation will be conducted to confirm the identity of the mineralization is, in fact, hydroxyapatite. Subsequent mechanical testing did not show the expected increase in structural rigidity in response to the mineralization. However, the extended soak time required for the mineralization process is expected to have degraded the scaffold and decreased its innate structural rigidity with the mineralization playing a key role in maintaining the scaffolds overall structural rigidity.

These results provide sufficient evidence to continue investigation into the efficacy of PPMS-DA hydrogels as a bone regenerative scaffold. Further studies will be conducted with a linear PDMS-MA to compare to PPMS-DA with constant crosslink density; diethyl vinylphosphonate to evaluate the osteoinductivity of the phosphonate without a siloxane backbone;

and a 25% phosphonate functionalized siloxane backbone to evaluate varying concentrations of phosphonate. Further materials characterization will be completed with non-templated hydrogels to better understand the fundamental material properties of the phosphonate containing hydrogels without the added sophistication of macropores. An additional area of interest is a real-time degradation study to further examine the degradation profile of the hybrid hydrogel scaffolds. Following the conclusion of materials characterization, cellular testing will be conducted to evaluate the cytotoxicity and osteogenic capacity of the hybrid hydrogel scaffolds.

REFERENCES

1. O'Brien, F. J., Biomaterials & scaffolds for tissue engineering. *Mater Today* **2011,** 14, (3), 88-95.

2. Vo, T. N.; Kasper, F. K.; Mikos, A. G., Strategies for controlled delivery of growth factors and cells for bone regeneration. *Adv Drug Deliv Rev* **2012,** 64, (12), 1292-1309.

3. Lutolf, M. P.; Hubbell, J. A., Synthetic biomaterials as instructive extracellular microenvironments for morphogenesis in tissue engineering. *Nature biotechnol* **2005,** 23, (1), 47-55.

4. Albrektsson, T.; Johansson, C., Osteoinduction, osteoconduction and osseointegration. *Eur Spine J* **2001,** 10 Suppl 2, S96-101.

5. Rezwan, K.; Chen, Q. Z.; Blaker, J. J.; Boccaccini, A. R., Biodegradable and bioactive porous polymer/inorganic composite scaffolds for bone tissue engineering. *Biomaterials* **2006,** 27, (18), 3413-3431.

6.Stevens, M. M., Biomaterials for bone tissue engineering. *Mater Today Chem* **2008,** 11, (5), 18-25.

7. Wang, W.; Yeung, K. W. K., Bone grafts and biomaterials substitutes for bone defect repair: a review. *Bioact Mater* **2017,** 2, (4), 224-247.

8. Hou, Y.; Schoener, C. A.; Regan, K. R.; Munoz-Pinto, D.; Hahn, M. S.; Grunlan, M. A., Photo-cross-linked PDMSstar-PEG hydrogels: synthesis, characterization, and potential application for tissue engineering scaffolds. *Biomacromolecules* **2010,** 11, (3), 648-656.

9. Zhu, J., Bioactive modification of poly(ethylene glycol) hydrogels for tissue engineering. *Biomaterials* **2010,** 31, (17), 4639-56.

10. Munoz-Pinto, D. J.; Jimenez-Vergara, A. C.; Hou, Y.; Hayenga, H. N.; Rivas, A.; Grunlan, M.; Hahn, M. S., Osteogenic potential of poly(ethylene glycol)–poly(dimethylsiloxane) hybrid hydrogels. *Tissue Eng Part A* **2012,** 18, (15-16), 1710-1719.

11. Bailey, B. M.; Fei, R.; Munoz-Pinto, D.; Hahn, M. S.; Grunlan, M. A., PDMS(star)-PEG hydrogels prepared via solvent-induced phase separation (SIPS) and their potential utility as tissue engineering scaffolds. *Acta Biomater* **2012,** 8, (12), 4324-33.

12. Gacasan, E. G.; Sehnert, R. M.; Ehrhardt, D. A.; Grunlan, M. A., Templated, macroporous PEG-DA hydrogels and their potential utility as tissue engineering scaffolds. *Macromol Mater Eng* **2017,** 302, (5), 1600512.

13. Murphy, C. M.; O'Brien, F. J., Understanding the effect of mean pore size on cell activity in collagen-glycosaminoglycan scaffolds. *Cell Adh Migr* **2010,** 4, (3), 377-381.

14. Watson, B. M.; Kasper, F. K.; Mikos, A. G., Phosphorous-containing polymers for regenerative medicine. *Biomed Mater* **2014,** 9, (2), 025014.

15. Kokubo, T.; Takadama, H., How useful is SBF in predicting in vivo bone bioactivity? *Biomaterials* **2006,** 27, (15), 2907-2915.

16. Rey, C.; Combes, C.; Drouet, C.; Glimcher, M. J., Bone mineral: update on chemical composition and structure. *Osteoporos Int* **2009,** 20, (6), 1013-1021.

17. Huebsch, N.; Arany, P. R.; Mao, A. S.; Shvartsman, D.; Ali, O. A.; Bencherif, S. A.; Rivera-Feliciano, J.; Mooney, D. J., Harnessing traction-mediated manipulation of the cell/matrix interface to control stem-cell fate. *Nat Mater* **2010,** 9, (6), 518-526.

18. Engler, A. J.; Sen, S.; Sweeney, H. L.; Discher, D. E., Matrix elasticity directs stem cell lineage specification. *Cell* **2006,** 126, (4), 677-89.

19. Ivirico, J. L.; Salmeron-Sanchez, M.; Ribelles, J. L.; Pradas, M. M.; Soria, J. M.; Gomes, M. E.; Reis, R. L.; Mano, J. F., Proliferation and differentiation of goat bone marrow stromal cells in 3D scaffolds with tunable hydrophilicity. *J Biomed Mater Res B, Appl Biomater* **2009,** 91, (1), 277-86.

20. Peters, F.; Epple, M., Crystallisation of calcium phosphates under constant conditions with a double diffusion set-up. *J Chem Soc, Dalton Trans* **2001**, (24), 3585-3592.

21. Vallet-Regí, M.; Romero, A. M.; Ragel, C. V.; LeGeros, R. Z., XRD, SEM-EDS, and FTIR studies of in vitro growth of an apatite-like layer on sol-gel glasses. *J Biomed Mater Research* **1999,** 44, (4), 416-421.

22. Dutta, R. C.; Dutta, A. K., Cell-interactive 3D-scaffold; advances and applications. *Biotechnol Adv* **2009,** 27, (4), 334-9.

23. Brandl, F.; Sommer, F.; Goepferich, A., Rational design of hydrogels for tissue engineering: impact of physical factors on cell behavior. *Biomaterials* **2007,** 28, (2), 134-46.

APPENDIX

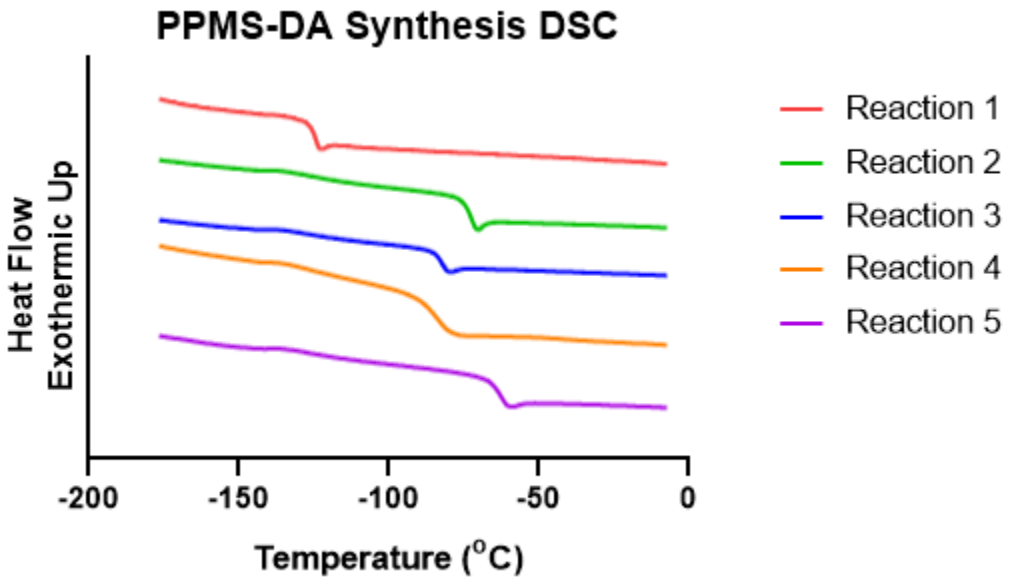

Figure A1: DSC data for each reaction involved in PPMS-DA synthesis. Reaction 1-5 corresponds to the products in the reactions mentioned in the Results and Discussion Polymer Synthesis section.

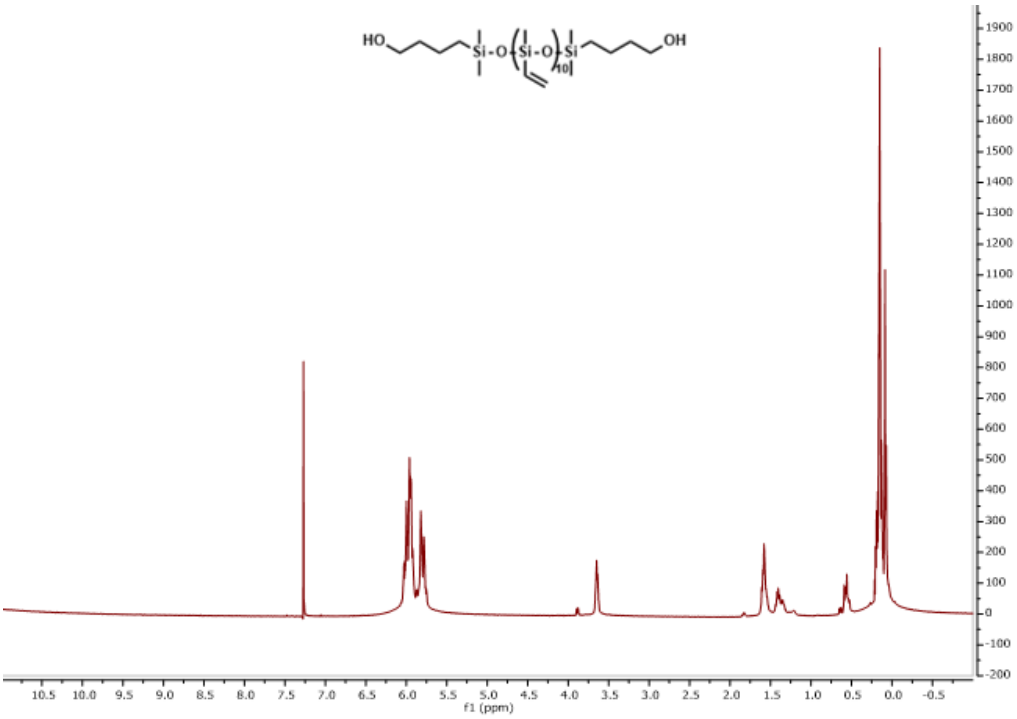

Figure A2: NMR corresponding to reaction 1 of PPMS-DA synthesis.

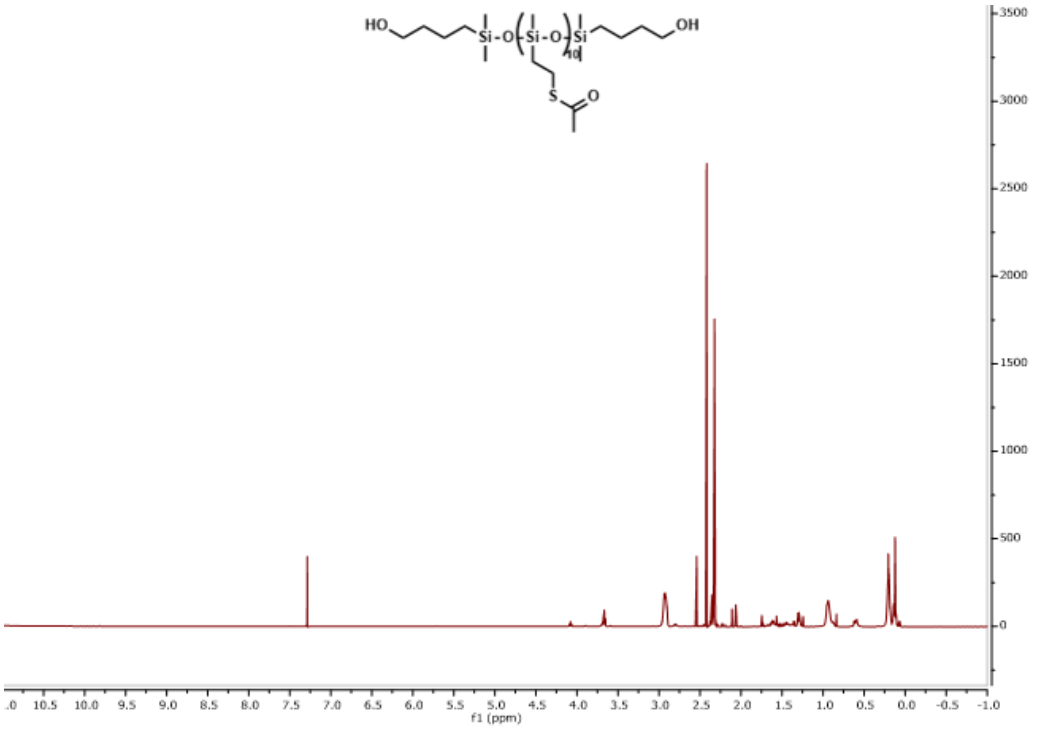

Figure A3: NMR corresponding to reaction 2 of PPMS-DA synthesis.

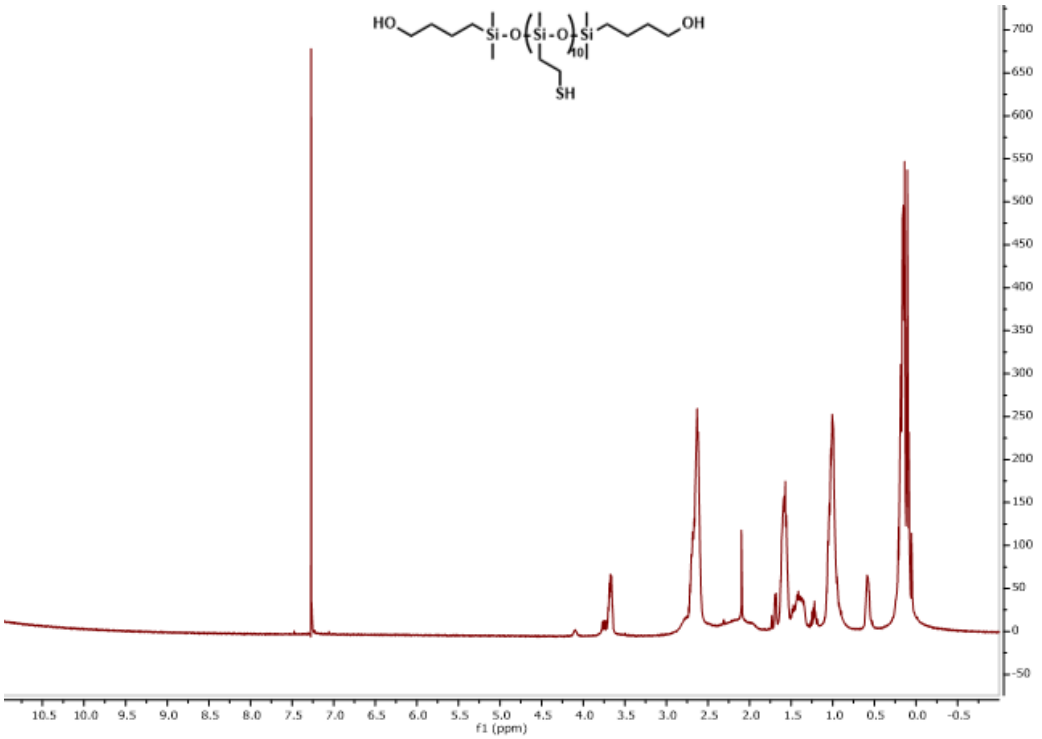

Figure A4: NMR corresponding to reaction 3 of PPMS-DA synthesis.

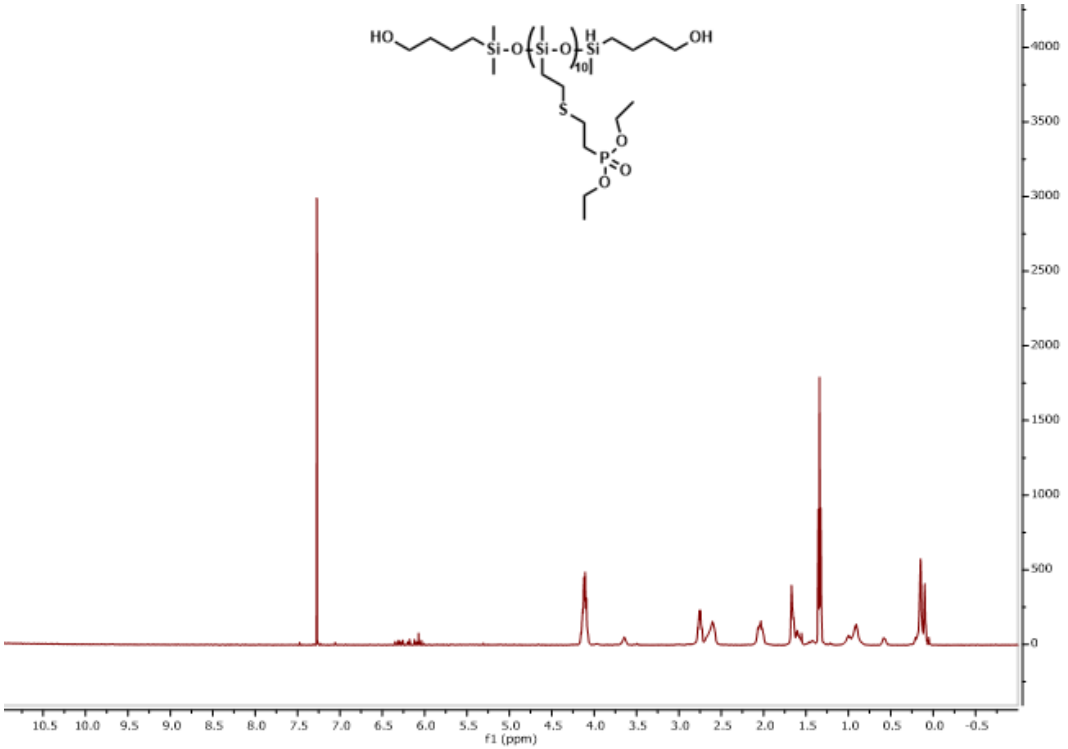

Figure A5: NMR corresponding to reaction 4 of PPMS-DA synthesis.

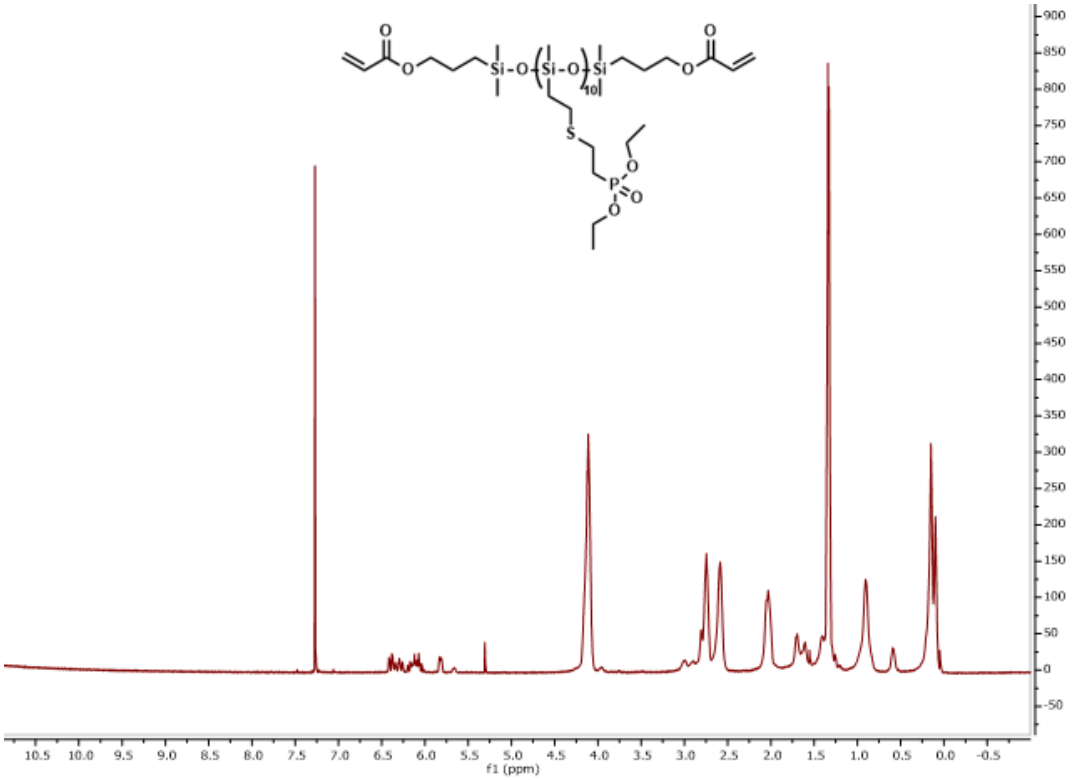

Figure A6: NMR corresponding to reaction 5 of PPMS-DA synthesis.

Table A1: Glass transition temperature for the product of each reaction involved in the PPMS-DA synthesis. Reaction 1-5 corresponds to the products in the reactions mentioned in the Results and Discussion Polymer Synthesis section.

Glass Transition Temperature				
Reaction 1	**Reaction 2**	**Reaction 3**	**Reaction 4**	**Reaction 5**
-124.12°C	-72.51°C	-82.14°C	-83.20°C	-62.36°C

Table A2: Sol content less than 5% verified successful crosslinking.

Sol Content				
PEG-DA	**PDMS$_{star}$-MA**	**PPMS 10:90**	**PPMS 20:80**	**PPMS 30:70**
4.14 ± 1.90%	2.41 ± 2.46%	0.82 ± 1.59%	2.72 ± 1.57%	3.67 ± 1.59%

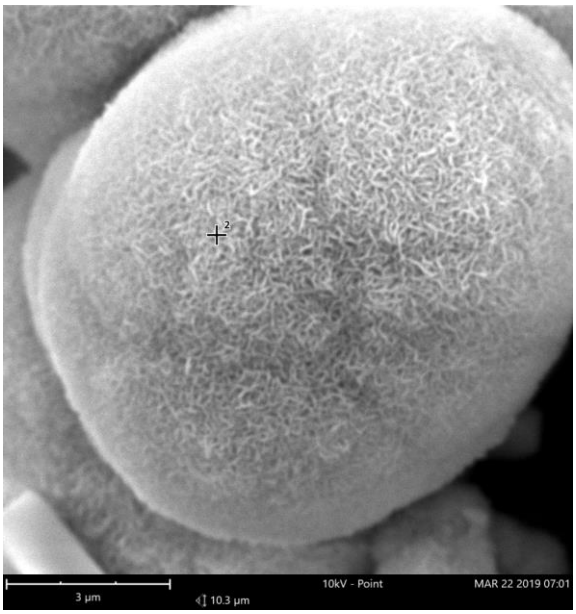

Figure A7: Mineralization topography was analyzed with SEM. Mineralization following SBF soak follows structural descriptions of hydroxyapatite. Scale bar = 3µm.